Ionospheric response over Thailand from the 15 January 2022 eruption of the Hunga Tonga-Hunga Ha'apai volcano

P. Jamlongkul[1,2,3,4], S. Wannawichian[2,3], L. J. Paxton[4], C. E. Cantrall[4], P. Supnithi[5], J. Budtho[5], M. Nishioka[6], T. Thanakulketsarat[5], and P. Thammavongsy[5]

[1]Ph.D. program in Physics, Department of Physics and Materials Science, Faculty of Science, Chiang Mai University, Chiang Mai, 50200, Thailand
[2]National Astronomical Research Institute of Thailand (Public Organization), Chiang Mai, 50180, Thailand
[3]Department of Physics and Materials Science, Faculty of Science, Chiang Mai University, Chiang Mai, 50200, Thailand
[4]Applied Physics Laboratory, Johns Hopkins University, Laurel, Maryland, 20723, USA
[5]School of Engineering, King Mongkut's Institute of Technology Ladkrabang, Bangkok, 10520, Thailand
[6]Space Environment Laboratory, Applied Electromagnetic Research Institute, National Institute of Information and Communications Technology, Tokyo, 183-8795, Japan

Key Points:

- Hunga Tonga-Hunga Ha'apai eruption caused ionospheric disturbances in Thailand 9 hours after the eruption with a wavefront speed of ∼275 m/s
- Two significant traveling ionospheric disturbance shock waves reached Thailand at 13 UT and 14 UT
- Equatorial plasma bubbles triggered by the eruption spread horizontally for 1000 km and vertically for 700 km were spotted in Thailand

Corresponding author: Paparin Jamlongkul, paparin_ja@cmu.ac.th

Corresponding author: Suwicha Wannawichian, suwicha.w@cmu.ac.th

Abstract

This study reports on the upper atmospheric response over Thailand to the Hunga Tonga volcano's eruption on January 15th, 2022. The eruption occurred during the geomagnetic storm recovery phase, providing a rare comparison between effects from outside (geomagnetic storm) and inside atmosphere (volcanic eruption). About nine hours later, we observed post-eruption fluctuations in the ionosphere total electron content (TEC). TEC was recorded in Thailand approximately ten times remarkably higher than typical levels from this large perturbation. The initial impact reached Thailand with speed of ∼275 m/s. Detrended TEC (dTEC) revealed mixed wave packets at various intervals. Two significant traveling ionospheric disturbance (TID) waves reached Thailand at 13 UT and 14 UT, respectively. Equatorial plasma bubbles (EPBs) were observed between 12-15 UT and 17-18 UT over Thailand. Our findings could provide insight into how communication signals over Thailand are affected by both disturbances, particularly in the case of widespread volcanic eruptions.

Plain Language Summary

The Hunga Tonga eruption had a significant impact on the upper atmosphere globally. This study investigates the eruption's impact on Thailand's ionosphere by comparing it to geomagnetic storm-induced changes preceding the volcanic eruption. Studying how waves moved through the atmosphere and changes in observable upper atmospheric phenomena, we found that substantial perturbations in total electron content, or TEC, are about ten times higher than usual. The first perturbation arrived over Thailand nine hours after the eruption, indicating a speed of approximately 275 meters per second. Mixed wave patterns also occurred at specific intervals throughout the day. Since the first wave packet appeared after the eruption, two large waves reached Thailand about four and five hours later, respectively. Additionally, ionospheric bubbles formed over Thailand that night. Overall, this analysis shows how the eruption's impact interacted with other atmospheric dynamics, highlighting the complexity of regional-scale changes in the ionosphere.

1 Introduction

The opportunity to investigate the consequences of both external (geomagnetic storm) and internal (geological activity) drivers, the case of the Hunga Tonga-Hunga Ha'apai (HTHH) volcanic eruption on January 15th, 2022, is unique. The HTHH volcano located at 20.54°S geographic latitude and 175.38°W geographic longitude in the South Pacific is particularly intriguing to be observed for the co-volcanic ionospheric disturbances (CVIDs) following the moderate geomagnetic storm (G2, Kp 6-) event influenced by a coronal mass ejection (CME) on January 14th, 2022. In addition, a minor geomagnetic storm (G1, Kp 5-) was produced at the end of the UT time on day 15th from the impact of a high-speed solar wind stream originating from a coronal hole (Aa et al., 2022). Generally, the energy from energetic particles during the geomagnetic storm event produces high-latitude heating, which can produce TIDs. The propagation of these waves is typically studied by deriving from TIDs, the detrended change in TEC (dTEC).

The eruption took place at ∼4:14 UT on January 15th, 2022, during the recovery phase of the January 14th geomagnetic storm. Previous studies in the Asian sector have reported TIDs (Pradipta et al., 2023; Rakesh et al., 2022; Li et al., 2023; Sun et al., 2022; Saito, 2022; Hong et al., 2022; Zhang et al., 2022; Astafyeva et al., 2022; Aa et al., 2022; Muafiry et al., 2022). The HTHH eruption and its aftermath (Tarumi & Yoshizawa, 2023) generated acoustic and gravity waves creating the Lamb waves over a wide range frequency (Astafyeva et al., 2022; Zhang et al., 2022) that spread globally for several days after the

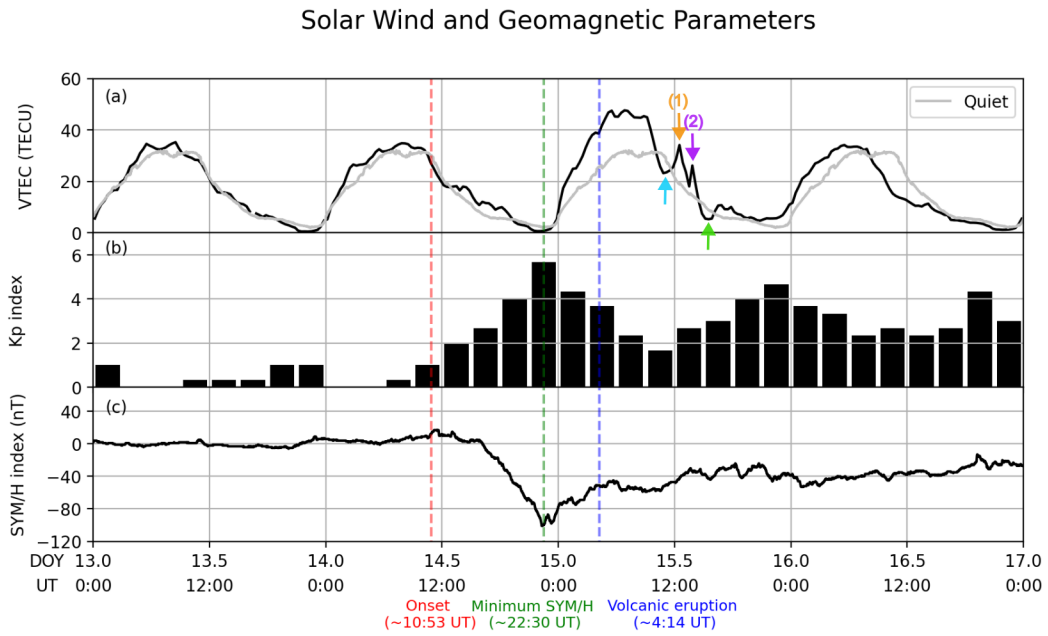

Figure 1. (a) VTEC and average VTEC during quiet phase (gray line) from KMI6 (Thailand station) shows the typical day-to-night variation found at this location, (b) Kp index, and (c) SYM/H index throughout January 13th-17th, 2022. The onset of the geomagnetic storm, occurring around 10:53 UT on January 14th, is marked by the red dashed line. The beginning of the recovery phase, indicated by the minimum SYM/H time around 22:30 UT on January 14th, is represented by the green dashed line. The volcanic eruption, occurring at approximately 4:14 UT on January 15th, is denoted by the blue dashed line. There is a sudden increase in VTEC after the SYM/H index reaches its minimum value. Two significant VTEC wavefronts arrive in Thailand. The initial and subsequent peak arrival times in Thailand are labeled with an orange arrow labeled (1) and a purple arrow labeled (2), respectively. Sky blue and green arrows indicate two troughs before the initial and after the subsequent peaks, respectively.

explosion. CVIDs often represent quasi-periodic variations of ionospheric electron density or TEC with periods of 12–30 minutes (Shults et al., 2016).

The Earth's ionospheric disturbances in low-latitude regions are known to be caused by sudden composition changes originating from external and internal sources. This work, focuses on the response over Thailand, indicating a growing interest in the field of ionospheric research in Thailand and filling in gaps in observations. These dynamic phenomena are crucial to understanding ionospheric behavior. An important ionospheric focus has been characterizing ionospheric gradients, waves, and plasma bubbles. The causes of the ionospheric gradients are varied and include traveling ionosphere disturbances (TIDs) and ionospheric irregularities (Liu et al., 2018). Ionospheric irregularities over Thailand are influenced by several factors, including solar activity, geomagnetic conditions, and local atmospheric dynamics, contributing to TEC variability and irregularities near the equatorial region. Moreover, ionospheric irregularities in Thailand primarily occur at night, with the appearance of spread F and pre-midnight scintillation inhibited by magnetic activity (Charoenkalunyuta et al., 2012). These irregularities can significantly affect radio wave propagation, satellite communications, and navigation systems.

2 Data and Method

This study investigates ionospheric irregularities using regional TEC data from the global navigation satellite system (GNSS) TEC data from the global Madrigal database and Thailand sites in Southeast Asia, which is near the equatorial region. The analysis period is particularly interesting because the observations reported here occurred during a geomagnetic disturbance and eruption of the Hunga Tonga volcano.

For regional data, the 1-second TEC and the 5-minute rate of TEC change index (ROTI) were obtained at Bangkok (KMI6: 13.77°, 100.53°) and Chumphon (CPN1: 10.76°, 99.37°) stations referenced to 350 km altitudes over Thailand (Bumrungkit et al., 2018). The slant measurements of TEC (STEC), derived from GNSS satellite ranging data observations, are converted to vertical TEC (VTEC) using the 350 km assumed pierce point location. The time variations of the VTEC from January 13th to 17th, 2022, were binned at 20-minute temporal resolution across a range of 5°× 5°in latitude and longitude of the Thailand region (black line in Figure 1a) in comparison with the average VTEC during the quiet phase from January 10th-12th, 2022 (gray line in Figure 1a). The distance-time of VTEC and ROTI in Thailand were calculated (Figures 3a and 3b). The phase speed is determined by analyzing the maximum VTEC within 20-minute and 200-kilometer intervals.

To process the data, we applied the Savitzky-Golay moving average method for calculating the dTEC (Savitzky & Golay, 1964; Astafyeva et al., 2022; Zhang et al., 2022; Sun et al., 2022; Li et al., 2023; Aa et al., 2022; Hong et al., 2022; Saito, 2022). The dTEC data were extracted from particular lines of sights (LOSs) corresponding to satellite paths from Hunga Tonga to Thailand during 7 UT to 21 UT (Figure 4). Subsequently, disturbed wave periods were identified using Lomb-Scargle periodogram analysis (Lomb, 1976; Scargle, 1982).

From more than 5000 stations, 5-minute VTEC data referenced to the 350-km pierce point altitude were obtained from the worldwide Madrigal GNSS database (http:- //millstonehill.haystack.mit.edu/). The global distance-time VTEC variations were calculated for ten latitude-longitude-distance bins from Tonga to Thailand along the great-arc circle (Figure 2). The propagation speed was based on the maximum VTEC within the mean 20-minute observation, using 52 minutes after the eruption until the first peak arrived in Thailand at around 12:30 UT.

Very High Frequency (VHF) radar (transmitting at 39.65 MHz) data were obtained from the Prachomklao VHF radar station at the King Mongkut's Institute of Technology Ladkrabang (KMITL) Chumphon campus, provided by the National Institute of Information and Communications Technology (NICT) and KMITL (Thanakulketsarat et al., 2023).

3 Results and Discussion

Figure 1 depicts temporal VTEC variations in the VTEC from the KMI6 station (located at 10° latitude and 100° longitude), alongside Kp and SYM/H indices for the period spanning from January 13th to 17th, 2022. This time duration covers varying conditions from quiet time through a geomagnetic storm event and up to a volcanic eruption (illustrated by the dashed blue line) during the geomagnetic storm recovery phase. The precise onset time (depicted by the dashed red line) of the moderate geomagnetic storm event on January 14th was difficult to determine due to a slight increase in the SYM/H index. We define the onset time as approximately 10:53 UT, based on a minor peak in the SYM/H index, reaching ∼17 nT, coinciding with the beginning of the rise in the Kp index. The initial and main phases of the geomagnetic storm each lasted around 5-6 hours. The recovery phase commenced with the first minimum in the SYM/H in-

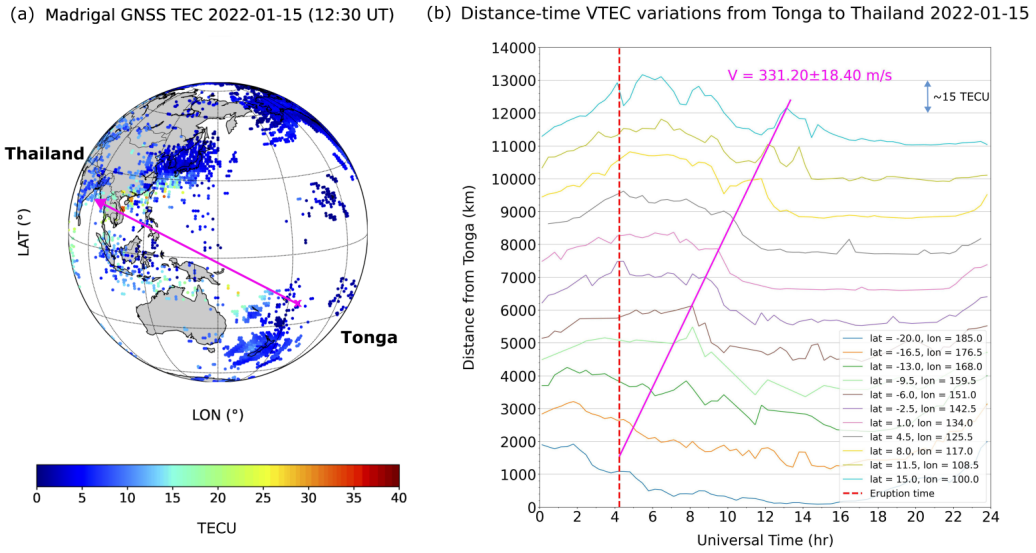

Figure 2. (a) VTEC at 12:30 UT from the worldwide Madrigal database. (b) The variations in VTEC across global distances, from Tonga to Thailand, at the time of the volcanic eruption around 4:14 UT, are represented by a red dashed line. The propagation speed along this distance-time VTEC trajectory from Tonga to Thailand is 313 m/s, as indicated by the solid magenta line in (a).

dex, ∼-100 nT, reaching a peak Kp index at around 22:30 UT on January 14th (indicated by the dashed green line).

Throughout the main phase of the geomagnetic storm, VTEC variations in Thailand remained relatively stable. However, following two occurrences of minimum SYM/H index values, coinciding with the highest Kp index readings between 21-23 UT on January 14th, significant increases in VTEC were observed during the daytime on January 15th, continuing through the time of the volcanic eruption. This suggests that the observed VTEC variations were primarily influenced by the geomagnetic storm rather than the volcanic eruption, given the propagation time. In this case, the observed VTEC increases at the KMI6 station indicate the occurrence of the ionospheric positive storm concurrent with the first minimum SYM/H index rather than during the main phase from 11-16 UT on January 14th.

Figure 2b illustrates the propagation at a speed of approximately 331 m/s since the HTHH eruption. The sharp increase in VTEC observed on the distance-time graph for the KMI6 and CPN1 stations indicates a front speed of ∼275 m/s (Figure 3a). This speed is lower than that derived from the global propagated direction. The VTEC observed farther away from HTHH, at approximately 10,000-km range (represented by the solid olive line in Figure 3b), corresponds to the VTEC observed by KMI6 in Thailand.

A trough of VTEC from the VTEC depletion (sky blue arrow in Figure 1a) occurred around 1.5 hours (∼11 UT) before the initial rise in VTEC observed in Thailand at around 12:30 UT (orange arrow (1) in Figure 1a). This first VTEC peak took ∼9 hours to arrive in Thailand after the volcanic eruption, consistent with findings from previous studies in nearby regions (Sun et al., 2022; Hong et al., 2022; Saito, 2022). A second VTEC peak occurred at ∼13:45 UT (purple arrow (2) in Figure 1a), followed by another trough of TEC at ∼15:30 UT (green arrow in Figure 1a). On January 16th, during the daytime, VTEC increased slightly earlier than the average observed during quiet conditions, likely

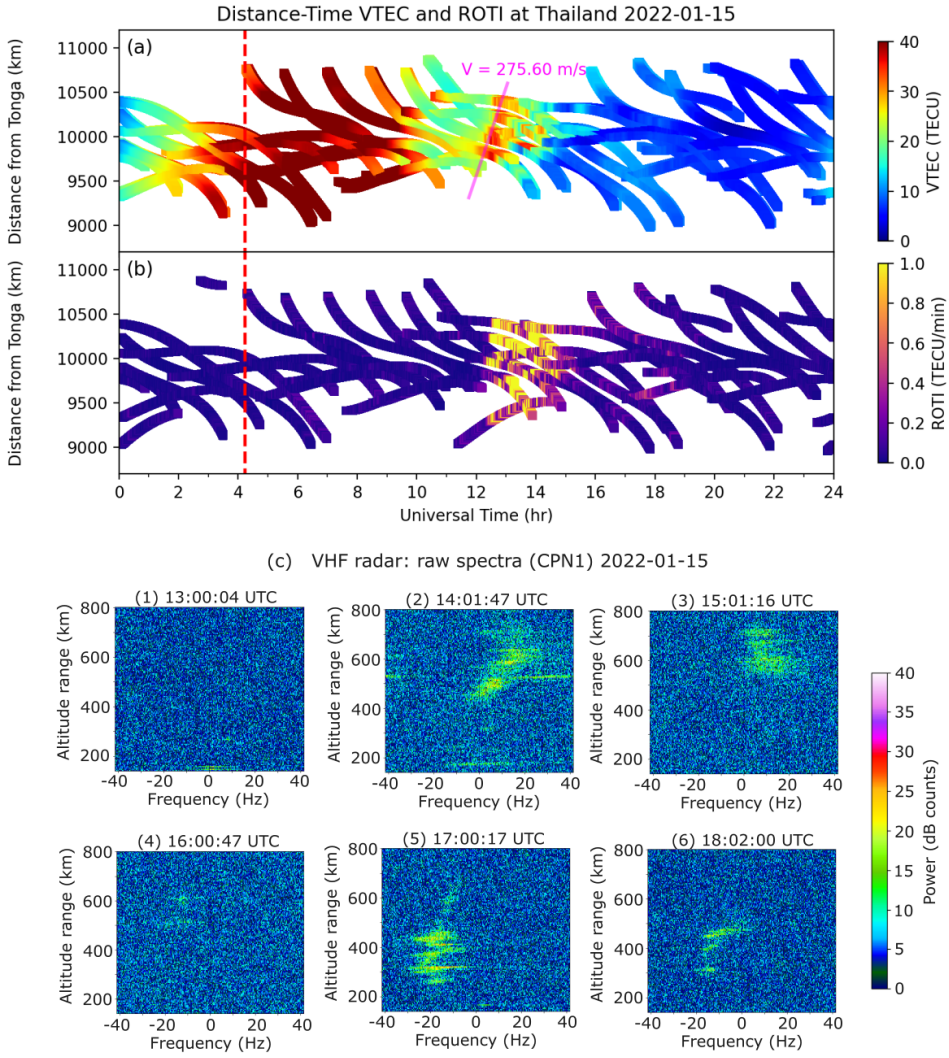

Figure 3. Distance-time variations from Tonga to Thailand were analyzed using data from KMI6 and CPN1 stations, showing: (a) VTEC with the propagation speed (magenta solid line) of sudden VTEC changed in Thailand, occurring around 275 m/s at approximately 9 hours after the HTHH volcanic eruption (red dashed line), and (b) ROTI displaying the expansion of EPBs horizontally over 1000-km range. (c) Spectra of VHF radar varying with altitudes measured by CPN1 station at (1) 13 UT, (2) 14 UT, (3) 15 UT, (4) 16 UT, (5) 17 UT, and (6) 18 UT. The EPB at 14 UT and 15 UT reaches altitudes up to 700 km, fades at 16 UT, and reappears again at 17 UT and 18 UT.

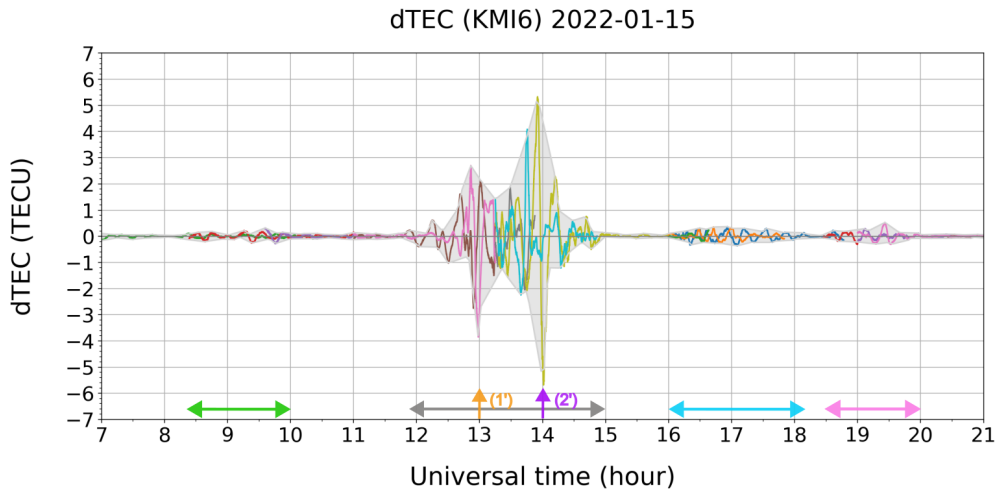

Figure 4. The dTEC along satellite's lines of sight in oriented directions from Hunga Tonga to Thailand. Mixed wave packets from 7 UT to 21 UT, occurring at various intervals: 8.5-10 UT (green double-head arrow), 12-15 UT (gray double-head arrow), 16-18 UT (sky blue double-head arrow), and 18.5-20 UT (pink double-head arrow). Between 12-15 UT, disturbances intensified around 12 UT, about 8 hours after the HTHH eruption. Fluctuations in dTEC peaked around 13 UT (orange arrow) and again at 14 UT (purple arrow), resembling TID shock waves. Intensity decreased after 15 UT.

due to residual enhanced VTEC levels. Subsequently, a decline in VTEC was observed, indicating diminishing volcanic impact, followed by a well-defined recovery phase.

The dTEC from 7 UT to 21 UT (illustrated in Figure 4) reveals mixed wave packets extracted along the satellite's lines of sight oriented from Hunga Tonga to Thailand at various intervals: 8.5-10 UT (green double-head arrow), 12-15 UT (gray double-head arrow), 16-18 UT (sky blue double-head arrow), and 18.5-20 UT (pink double-head arrow). During the 12-15 UT interval, these disturbances began intensifying around 12 UT, approximately 8 hours after the eruption of HTHH. The sudden fluctuations in dTEC, ranging between 1-3 TECU around 13 UT (referred to the orange arrow (1') in Figure 4), demonstrated a significant increase, resembling a TID shock wave. This coincides with the first peak of VTEC arrival in Thailand, occurring at approximately 12:30 UT (marked by the orange arrow (1) in Figure 1a), before gradually diminishing.

Around 14 UT, another significant increase in dTEC occurred, indicating the arrival of another significant TID shock wave (referred to as purple (2') in Figure 4), corresponding to the sudden fluctuations of the second peak of VTEC at ∼13:45 UT (purple arrow (2) in Figure 1a). These fluctuations gradually diminish in intensity from 15 UT onwards, showing only small variations thereafter. This second disturbance decayed more rapidly, resembling the rate of decay observed in the first wave packet. Other small ionospheric conditions remained significantly disturbed for several hours, with background disturbances persisting until returning to normal storm-time conditions over Thailand.

At a distance of 10,000-km range, we noted three occurrences where the dTEC envelopes correspond with Zhang et al. (2022) during the same time intervals. Specifically, wave packet (1') corresponds to the dTEC arrival time (∼13 UT) for wave travel along the great circle route at a velocity of 350 m/s, while wave packet (2') corresponds to the

dTEC arrival time (∼14 UT) for wave travel along the great circle route at a velocity of 300 m/s. Additionally, the dTEC observed in the interval 8.5-10 UT, 16-18 UT, and 18.5-20 UT could be associated with observing other medium-scale TID (MSTID) with the 20-minute wave period. However, this TID dissipated quickly due to its rapid velocity. The faster wave would have already reached the 10,000 km mark because it diminishes more rapidly.

During 12-15 UT on January 15th, a high level of variation in the distance-time profile of ROTI (KMI6) (Figure 3b) was observed over a horizontal distance of more than 1000 km. The changes in ROTI demonstrated fluctuations, indicating the presence of equatorial plasma bubbles (EPBs) over Thailand, consistent with the observations of EPB "C" reported by Sun et al. (2022). The hourly VHF radar (CPN1) (Figure 3c) also presents the formation dynamics of EPBs. Discrepancies between the VHF radar data and ROTI were observed. It could be due to differences in observation locations or the propagation characteristics of EPBs. Spatial expansion at very high altitudes, up to approximately 700 km, was noted at 14 UT (Figure 3c-2) and 15 UT (Figure 3c-3) based on spectral data analysis. Consequently, the EPBs disappeared but reassembled around 16 UT (Figure 3c-4) at different locations, suggesting the formation of new EPBs during the recovery phase between 17-18 UT (Figures 3c-5 and 3c-6).

4 Summary

The data collected from Thai stations highlighted substantial deviations from the usual ionospheric conditions attributed to moderate and minor geomagnetic storm drivers and a volcanic eruption. Disturbances observed on January 15th, characterized by a significant increase in VTEC, were typical of geomagnetic storms. However, unusual horizontal wave-like perturbations in dTEC, commencing around 9 hours after the eruption, were related to volcanic activity. Two significant TID shock waves reached Thailand at 13 UT (350 m/s) and 14 UT (300 m/s), respectively, lasting about 3 hours. The observed VTEC depletion on January 16th confirmed the impact of geomagnetic storm activity during the recovery phase in low-latitude regions. On this day, distinct EPBs were observed on a large scale, spanning over 1000 km horizontally and up to 700 km in altitude. These EPBs appear to have been produced by the HTHH eruption. In the future, the formations of EPBs resulting from the volcanic eruption, particularly compared to those arising during the main phase of geomagnetic storm events, should be further investigated. Additional data from diverse stations, incorporating information or relevant events or aftermath effects of the explosion, is essential to comprehensively analyze these phenomena. Moreover, this event holds significance for understanding disruptions caused by external and internal energy sources, with potential implications for future communication signal impacts.

Open Research

The solar wind parameters and the geomagnetic indices are obtained by NASA/GSFC's Space Physics Data Facility's OMNIWeb service (https://omniweb.gsfc.nasa.gov/), and the World Data Center for Geomagnetism, Kyoto (https://wdc.kugi.kyoto-u.ac.jp/). The SuperMAG collaborators (https://supermag.jhuapl.edu/info/?page=acknowledgement) provide AE index data. The Kp index is available from GFZ German Research Centre for Geosciences (https://kp.gfz-potsdam.de/en/data). The KMI6 and CPN1 GNSS data are provided by the Thai GNSS and Space Weather Information Data Center hosted at King Mongkut's Institute of Technology Ladkrabang (KMITL), Thailand (http://iono-gnss.kmitl.ac.th). The worldwide GNSS data are available from the CEDAR Madrigal database (http:// cedar.openmadrigal.org/). The VHF data are contributed from the Southeast Asia Low-latitude IOnosphere Network (SEALION) under the National In-

stitute of Information and Communications Technology (NICT) service (https://aer-nc-web.nict.go.jp/sealion/index.html).

Acknowledgments

This research project was supported by Fundamental Fund 2024, Chiang Mai University. Special thanks for the Development and Promotion of Science and Technology Talents Project (DPST) scholarship, Royal Government of Thailand. We acknowledge the Chalawan High Performance Computing (HPC) Cluster from the National Astronomical Research Institute of Thailand (NARIT).

References

Aa, E., Zhang, S.-R., Wang, W., Erickson, P. J., Qian, L., Eastes, R., ... Spicher, A. (2022). Pronounced suppression and x-pattern merging of equatorial ionization anomalies after the 2022 tonga volcano eruption. , *127*(6), e2022JA030527. doi: 10.1029/2022JA030527

Astafyeva, E., Maletckii, B., Mikesell, T. D., Munaibari, E., Ravanelli, M., Coisson, P., ... Rolland, L. (2022). The 15 january 2022 hunga tonga eruption history as inferred from ionospheric observations. , *49*(10), e2022GL098827. doi: 10.1029/2022GL098827

Bumrungkit, A., Supnithi, P., & Saito, S. (2018). Statistical analysis of separation distance between equatorial plasma bubbles near suvarnabhumi international airport, thailand. , *123*(9), 7858–7870. doi: 10.1029/2018JA025612

Charoenkalunyuta, T., Satirapod, C., Lee, H.-K., & Choi, Y.-S. (2012). Performance of network-based RTK GPS in low-latitude region: A case study in thailand. , *16*(5), 95–104. doi: 10.4186/ej.2012.16.5.95

Hong, J., Kil, H., Lee, W. K., Kwak, Y.-S., Choi, B.-K., & Paxton, L. J. (2022). Detection of different properties of ionospheric perturbations in the vicinity of the korean peninsula after the hunga-tonga volcanic eruption on 15 january 2022. , *49*(14), e2022GL099163. doi: 10.1029/2022GL099163

Li, X., Ding, F., Yue, X., Mao, T., Xiong, B., & Song, Q. (2023). Multiwave structure of traveling ionospheric disturbances excited by the tonga volcanic eruptions observed by a dense GNSS network in china. , *21*(2), e2022SW003210. doi: 10.1029/2022SW003210

Liu, Y., Fu, L., Wang, J., & Zhang, C. (2018). Studying ionosphere responses to a geomagnetic storm in june 2015 with multi-constellation observations. , *10*(5), 666. doi: 10.3390/rs10050666

Lomb, N. R. (1976). Least-squares frequency analysis of unequally spaced data. , *39*(2), 447–462. doi: 10.1007/BF00648343

Muafiry, I. N., Meilano, I., Heki, K., Wijaya, D. D., & Nugraha, K. A. (2022). Ionospheric disturbances after the 2022 hunga tonga-hunga ha'apai eruption above indonesia from GNSS-TEC observations. , *13*(10), 1615. doi: 10.3390/atmos13101615

Pradipta, R., Carter, B. A., Currie, J. L., Choy, S., Wilkinson, P., Maher, P., & Marshall, R. (2023). On the propagation of traveling ionospheric disturbances from the hunga tonga-hunga ha'apai volcano eruption and their possible connection with tsunami waves. , *50*(6), e2022GL101925. doi: 10.1029/2022GL101925

Rakesh, V., Haridas, S., Sivan, C., Manoj, M. G., Abhilash, S., Paul, B., ... Sumesh Chandran, R. (2022). Impact of the hunga tonga-hunga ha'apai volcanic eruption on the changes observed over the indian near-equatorial ionosphere. , *70*(8), 2480–2493. doi: 10.1016/j.asr.2022.07.004

Saito, S. (2022). Ionospheric disturbances observed over japan following the eruption of hunga tonga-hunga ha'apai on 15 january 2022. , *74*(1), 57. doi: 10.1186/

s40623-022-01619-0

Savitzky, A., & Golay, M. (1964). Smoothing and differentiation of data by simplified least squares procedures. , *36*(8), 1627–1639. doi: 10.1021/ac60214a047

Scargle, J. D. (1982). Studies in astronomical time series analysis. II. statistical aspects of spectral analysis of unevenly spaced data. , *263*, 835–853. doi: 10.1086/160554

Shults, K., Astafyeva, E., & Adourian, S. (2016). Ionospheric detection and localization of volcano eruptions on the example of the april 2015 calbuco events. , *121*(10), 10,303–10,315. doi: 10.1002/2016JA023382

Sun, W., Kuriakose, A. K., Li, G., Li, Y., Zhao, X., Hu, L., ... Liu, L. (2022). Unseasonal super ionospheric plasma bubble and scintillations seeded by the 2022 tonga volcano eruption related perturbations. , *12*, 25. doi: 10.1051/swsc/2022024

Tarumi, K., & Yoshizawa, K. (2023). Eruption sequence of the 2022 hunga tonga-hunga ha'apai explosion from back-projection of teleseismic p waves. , *602*, 117966. doi: 10.1016/j.epsl.2022.117966

Thanakulketsarat, T., Supnithi, P., Myint, L. M. M., Hozumi, K., & Nishioka, M. (2023). Classification of the equatorial plasma bubbles using convolutional neural network and support vector machine techniques. , *75*(1), 161. doi: 10.1186/s40623-023-01903-7

Zhang, S.-R., Vierinen, J., Aa, E., Goncharenko, L. P., Erickson, P. J., Rideout, W., ... Spicher, A. (2022). 2022 tonga volcanic eruption induced global propagation of ionospheric disturbances via lamb waves. , *9*.